Dynamics and Kinetics of Heat Transfer at the Interface of Model Diamond {111} Nanosurfaces†

Oleg A. Mazyar and William L. Hase*

Department of Chemistry and Biochemistry, Texas Tech University, Lubbock, Texas 79409-1061

Received: April 27, 2005; In Final Form: July 5, 2005

A molecular dynamics simulation was performed to study the effect of an applied force on heat transfer at the interface of model diamond {111} nanosurfaces. The force was applied to a small, hot nanosurface at 800, 1000, or 1200 K brought into contact with a larger, colder nanosurface at 300 K. The relaxation of the initial nonequilibrium interfacial force occurs on a subpicosecond time scale, much shorter than that required for heat transfer. Heat transfer occurs with exponential kinetics and a rate constant that increases linearly with the interfacial force according to 7×10^{-4} ps^{-1}/nN. This rate constant only increases by at most 10% as the temperature of the hot surface is increased from 800 to 1200 K. Replacing the interfacial H-atoms on both surfaces by D atoms also has a very small effect on the heat transfer. However, if one nanosurface has H atoms on its interface and the other nanosurface's interface has D atoms, then there is a marked 25% decrease in the rate constant for heat transfer. Increasing the size of the hot surface, and, thus, the interfacial contact area, increases the rate of heat transfer but not the rate constant. For the same interfacial force, different anharmonic models for the nanosurfaces' potential energy function give the same heat transfer rate constant. The possibility of quantum effects for heat transfer across the diamond interface is considered.

I. Introduction

There is considerable interest in obtaining a unified atomic-level understanding of fundamental properties that influence the rate of vibrational energy flow in molecules,[1−5] clusters,[6] liquids,[7,8] solids,[9,10] interfaces,[11,12] and nanomaterials.[13] Vibrational energy flow in molecules, that is, intramolecular vibrational energy redistribution (IVR),[1−5] has been studied for molecules ranging in size from benzene[14−17] and substituted methanes[18] to large macromolecules.[19−21] A cluster often has multiple potential energy minima and the efficiency of IVR affects its ability to access these minima.[22−25] Vibrational energy flow for a liquid includes IVR within solute molecules as well as energy flow from individual solute molecules to solvent molecules and intermolecular degrees of freedom.[7,8] Although disorder, that is, inhomogeneity, often localizes vibrational energy and restricts its flow in solids, vibrational energy flow may also be restricted in perfectly periodic systems through the presence of intrinsic localized modes (ILMs).[9] Understanding the origin and properties of these ILMs is an active area of research.[26] Energy flow at interfaces has been investigated by studying energy transfer as rare gas atoms collide with surfaces[27,28] and as two surfaces "rub" during sliding contact.[11,29] The nature of the vibrational modes and resulting vibrational energy flow for a nanomaterial may depend on the material's size. This effect was documented recently in experimental measurements of the C−H stretching infrared spectrum for diamond nanocrystals of different sizes.[13]

It is important to understand fundamental properties of vibrational energy transfer at the interface of nanoscale materials and devices. For a small component sliding across a much larger component of a microelectromechanical system (MEMS), heat transfer at the components' interface is an integral attribute of the device's properties and integrity. As a result of inhomogeneities at the interface and the interface's nanoscale attributes, the rate of heat transfer from the smaller to larger component is expected to be different than that for either of the components in a homogeneous macroscopic environment.[30] For macroscopic materials, heat transfer is impeded by interfacial roughness and a resulting small contact area.[31−34] For nanoscale materials, the efficiency of heat transfer is expected to also depend on atomic-level properties such as the interfacial intermolecular potential and the structures and vibrational frequencies of the two components.

Molecular dynamics (MD) simulations are an important means to obtaining an atomic-level description of energy transfer at the interface of nanosurfaces.[12] In previous MD simulations, nanoscale heat dissipation was investigated as part of the friction generated at the interface of two surfaces in sliding contact.[11,35−39] A technological important material studied in these simulations is diamond, and Harrison and co-workers[36−39] have identified numerous excitation modes (rotation, turnstile, etc.) by which friction energy generated during the sliding of H- and alkyl-terminated diamond {111} surfaces is dissipated into the bulk as heat. A number of experimental studies[40−49] have also focused on identifying mechanisms for heat transfer and dissipation at nanoscale interfaces.

The standard MD simulation time is 10^{-9} s or shorter and the above simulations have focused on short-time relaxations that occur for fast sliding velocities. Some experiments have used fast sliding velocities of the order of 1 m/s or faster;[50] however, for most cases the sliding velocity is much slower as represented by 10^{-6} m/s or less for a typical atomic force microscopy (AFM) study.[43,45,51] For a 10^{-6} m/s sliding velocity and 10^{-9} s simulation, the system moves only 10^{-5} Å so that the surfaces are essentially static and do not move during the simulation. Thus, to simulate short-time relaxations, for tribology experiments with standard low sliding velocities, it is unneces-

† Part of the special issue "Donald G. Truhlar Festschrift".

* Corresponding author. E-mail: bill.hase@ttu.edu.

10.1021/jp0521961 CCC: $33.50
Published on Web 11/02/2005

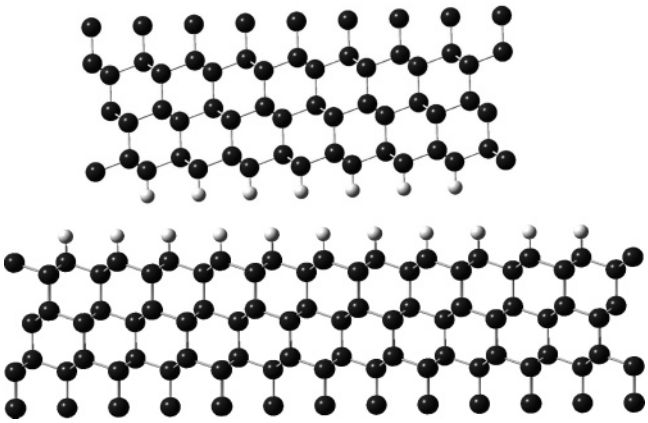

Figure 1. The diamond {111} surface and interface viewed along the [110] direction. Large dark-grey spheres represent carbon atoms and small light-grey spheres represent hydrogen atoms.

sary to slide the molecular system, and this is the approach used for simulations reported here.

The unique structural, electrical, and optical properties of diamond, and its wide use in optical windows, capacitors, abrasives, and heat exchangers, make the heat transfer within diamond nanosystems of particular interest.[52] In the work reported here, the dynamics of energy transfer at the interface of a small, hot nanoscale H-terminated diamond {111} surface and a much larger, colder identical surface were investigated by MD simulations. The rate constants for energy transfer from the hot to cold surface and the temperature gradients within each surface were determined. This energy transfer was simulated as a function of the force applied to the small surface, the initial temperature difference between the two surfaces, the interfacial contact area of the two surfaces, and alterations in the isotopic composition of the interface. Because of the weak van der Waals interaction between the two diamond surfaces, the application of an external applied force has a substantial effect on the efficiency of energy transfer across the surfaces' interface.

II. Computational Procedure

A. Surface Model and Potential Energy Function. Energy transfer was studied at the interface of two H-terminated {111} crystal faces of diamond (see Figure 1). For the potential energy minimum of each diamond lattice, the carbon atoms are assumed to conform to an exact tetrahedral bonding pattern. The carbon atoms are bonded in nonplanar hexagon structures, similar to the chair conformation of cyclohexane, in both the vertical and horizontal directions with respect to the surface interface. Figure 1 illustrates the hexagon structure for a vertical direction from the interface and shows that this hexagon structure results in carbon atoms arranged in layers, with two layers close together and separated by a greater distance from the next group of two layers. The surface of each lattice consists of hydrogen atoms bound to the outermost layer of carbon atoms.

The model used to study energy transfer at the interface is shown in Figure 2. It consists of an upper surface which, at 0 K, has a height of 19.65 Å and an interfacial area of 20.19 × 21.86 Å^2. The bottom surface has the same height, but a larger area of 60.58 × 65.59 Å^2. Each surface consists of twenty layers, that is, nineteen carbon and one hydrogen. The outermost layer of each surface is held rigid, with the relative separation of these two layers specifying the normal load applied to the surfaces.

The potential energy function for the system is written as a sum of potentials for the upper and lower surfaces, $V_{surf,u}$ and

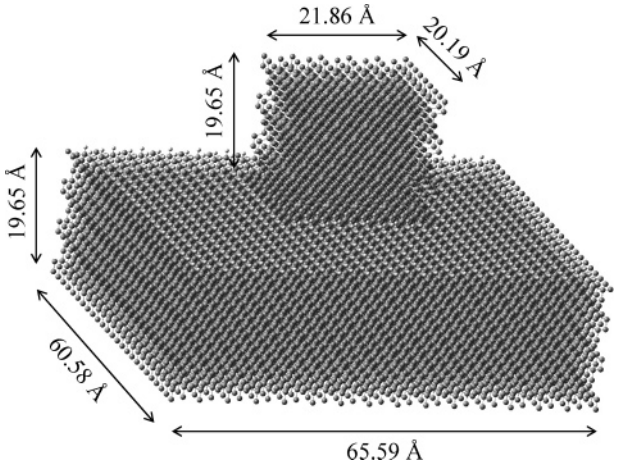

Figure 2. Depiction of the upper (hot) and larger, lower (cold) H-terminated {111} diamond surfaces. The dimensions of each surface are for their 0 K, equilibrium geometries.

$V_{surf,l}$, and the surface/surface intermolecular potential, V_{inter}:

$$V = V_{surf,u} + V_{surf,l} + V_{inter} \quad (1)$$

Three different models were used for V_{surf} to determine the sensitivity of the simulation results to the degree of anharmonicity in this potential. For the majority of the simulations, V_{surf} is the harmonic valence force field potential developed by Tubino et al.[53,54] to fit the diamond phonon spectrum, with the modification that the C−C and C−H stretches are represented by the Morse function,[55] that is, the following function for the C−C stretch

$$V(R) = D_R\,[1 - \exp\{-\beta_R(R - R_0)\}]^2 \quad (2)$$

In this function, D_R is the tertiary C−C bond dissociation energy of 79.46 kcal/mol and $\beta_R = (f_R/2D_R)^{1/2} = 1.858$ Å^{-1} was determined from the harmonic force constant, f_R, of 3.812 mdyn/Å. R_0 is equal to 1.54452 Å. Similarly, the C−H stretch potentials are Morse functions with $D_r = 104.94$ kcal/mol, $\beta_r = 1.852$ Å^{-1}, and $r_o = 1.09545$ Å. This surface potential is identified as Model 1 and its parameters are given in Table 1. This type of potential energy function, with Morse stretches and quadratic forces for the remaining potential terms, gives a relaxation rate for the $n = 3$ C−H overtone state of benzene, which agrees with experiment.[15−17]

Two additional surface potentials were used to investigate how varying the surface anharmonicity affects energy transfer. For Model 2, the Morse anharmonicity of the C−C and C−H stretches was retained and additional anharmonicity was introduced by attenuating the diagonal bending and nondiagonal stretch−bend and bend−bend quadratic force constants as a bond defining the potential term is stretched. This force constant attenuation by bond stretching is represented by

$$f(r) = f^\circ \qquad r \le r_o \quad (3)$$

$$f(r) = f^\circ \exp[-a(r - r_o)^2] \qquad r > r_o$$

Here f° is the diagonal bend, nondiagonal stretch−bend, or nondiagonal bend−bend quadratic force constant. The attenuation parameter was set to 1.00 Å^{-2}, a representative value for hydrocarbons.[56,57] The effect of this attenuation is to introduce cubic and higher order anharmonic terms to the potential and to ensure that the force constant properly goes to zero as a bond defining the potential term is elongated.

TABLE 1: Potential Energy Parameters

parameters for the H-terminated {111} surface[a]	
C−C stretch Morse function	
D_R	79.46 kcal/mol
β_R	1.858 Å^{-1}
R_0	1.54452 Å
C−H stretch Morse function	
D_r	109.94 kcal/mol
β_r	1.852 Å^{-1}
r_0	1.09545 Å
diagonal quadratic potential parameters	
θ_0	109.471°
φ_0	109.471°
f_θ	0.868 mdyn Å/rad^2
$f\varphi$	0.725 mdyn Å/rad^2
nondiagonal quadratic potential parameters	
$f_{R\bar{R}}$	0.163 mdyn/Å
$f_{R\theta}$	0.39 mdyn/rad
$f_{\theta\theta}$ [b]	0.177 mdyn Å/rad^2
$f_{\theta\bar{\theta}}$ [c]	−0.0149 mdyn Å/rad^2

parameters for the surface−surface intermolecular potential[d]

	a	*b*	*c*
H···H	2790.87	3.74	−32.50
H···C	15651.29	3.67	−136.95
C···C	87774.86	3.60	−576.96

[a] The coordinates R, r, θ, and φ are C−C stretch, C−H stretch, C−C−C bend, and C−C−H bend, respectively. [b] Nondiagonal force constant for two different C−C−C bends, which share one stretch coordinate but not a central atom. [c] Nondiagonal force constant for two different C−C−C bends, which share one stretch coordinate and a central atom. [d] The intermolecular potential energy parameters a, b, and c are in units of kcal/mol, Å^{-1}, and kcal Å^6/mol, respectively.

For the remaining potential, Model 3, the anharmonic Morse potentials of Model 1 for the C−C and C−H stretches were replaced by their harmonic analogues with f_R of 3.812 and f_r of 5.001 mdyn/Å so that the surface potential is completely quadratic with no anharmonic terms. Although this potential model is quadratic, the Hamiltonian for each lattice is harmonic and separable only for small displacements. For noninfinitesimal displacements, there are nonlinear terms in the Hamiltonian that couple the modes.[58] Also, the normal load applied to the surfaces will introduce couplings and anharmonicities.

V_{inter} in eq 1 describes the nonbonded intermolecular potential between the top and bottom surfaces. Only interactions between the terminal H-atoms and the C atoms of the first and second interfacial layers of the two surfaces are included in V_{inter} because the distances between other interfacial atoms are too large to contribute to $V_{\text{inter.}}$ These nonbonded H−H, C−H, and C−C potentials are represented by the EXP-6 function of Williams and Starr,[59] that is

$$V(r) = a\exp(-br) + \frac{c}{r^6} \tag{4}$$

which were derived to represent nonbonded interactions for hydrogen and carbon atoms in experimentally determined crystal structures of 18 hydrocarbon molecules. The parameters for the H−H, C−H, and C−C intermolecular potentials are listed in Table 1.

B. Molecular Dynamics Simulation. The VENUS computer program was used to perform the MD simulations.[60] Hamilton's equations were solved to determine the motion of the atoms in the nanosurfaces. The numerical integrations were initiated with a Runge−Kutta−Gill algorithm and then completed with a sixth-order Adams−Moulton routine.

In the simulations, heat transfer from the hot, upper surface to the cold, lower surface was studied as a function of applied force. The carbon atoms of the outermost layer of each surface were held rigid to maintain a fixed distance between the two surfaces, specified by the applied force. The two lowest C-atom layers of the bottom surface (excluding the outermost layer) were connected to a 300 K Berendsen thermal bath[61] during the numerical simulations. This bath provides a constant temperature thermostat, withdrawing heat from the lower surface as it is transferred from the upper surface.

A MD simulation was performed, with all nonrigid atoms of the surface connected to two Berendsen baths at the desired temperature, to equilibrate each of the nanosurfaces. This simulation was continued until the potential and kinetic energies of the nanosurface become equal. One thermal bath was coupled to the surface's carbon atoms and the other was connected to the hydrogen atoms to ensure rapid thermal equilibration of the surface at the given temperature because energy exchange between the C−H stretch modes and the other surface modes is a slow process. After this equilibration step, the upper surface was further equilibrated for 10 ps to ensure that the temperatures of the individual surface layers are the same and equal to the desired temperature. The temperature of the atoms in a layer was calculated by dividing the total kinetic energy of the layer's atoms by $3Nk_{\text{B}}$, where N is the number of atoms in the layer and k_{B} is Boltzmann's constant. The bottom surface was further equilibrated in the same manner for 30 ps to ensure that each of its surface layers are 300 K. For this step, the lowest two C-atom layers (excluding the outermost rigid layer) are connected to a 300 K Berendsen thermal bath because this bath is included in the simulation of heat transfer from the hot, upper to the cold, lower nanosurface (see above).

After the thermal equilibrations of the hot, upper and cold, lower surfaces were completed, these two surfaces were brought into contact so that the hydrogen atoms of one surface were centered over the second-layer carbon atoms of the other surface and the outer C-atom layers of the surfaces were separated by a specified distance. The nonbonded interactions between the interfacial layers of the hydrogen and carbon atoms of the two surfaces were then turned on, and a 52.5 ps simulation of energy transfer from the hot to cold diamond nanosurface was performed.

III. Simulation Results

A. Interfacial Separation. As described above, the outermost layers of the hot, upper and cold, lower surfaces are held fixed. The coordinate system used for the simulations places these outermost layers in the x,y plane, with their separation given by the distance between these planes in the z dimension. Fixing the separation between these outermost layers also defines the distance, S, between the planes of the interfacial H-atom layers. When each surface is in its 0 K equilibrium geometry, this resulting distance is identified as S_{eq}. Figure 3a gives a plot of the surfaces' interfacial intermolecular potential, V_{inter}, eq 1, as a function of $S_{\text{eq.}}$ Each surface is held in its equilibrium geometry in calculating this potential energy curve. The resulting force, that is, the interfacial force, is the derivative of V_{inter} with respect to S_{eq} and is plotted in Figure 3b as a function of S_{eq}.

The value of S for the simulations is larger than S_{eq} because of the repulsive interaction at the interface. Simulations were performed with a 300 K temperature for each surface to determine the value of S after the surfaces had equilibrated. These simulations were performed with potential Model 1, H atoms at the interface, the small interfacial area for the upper

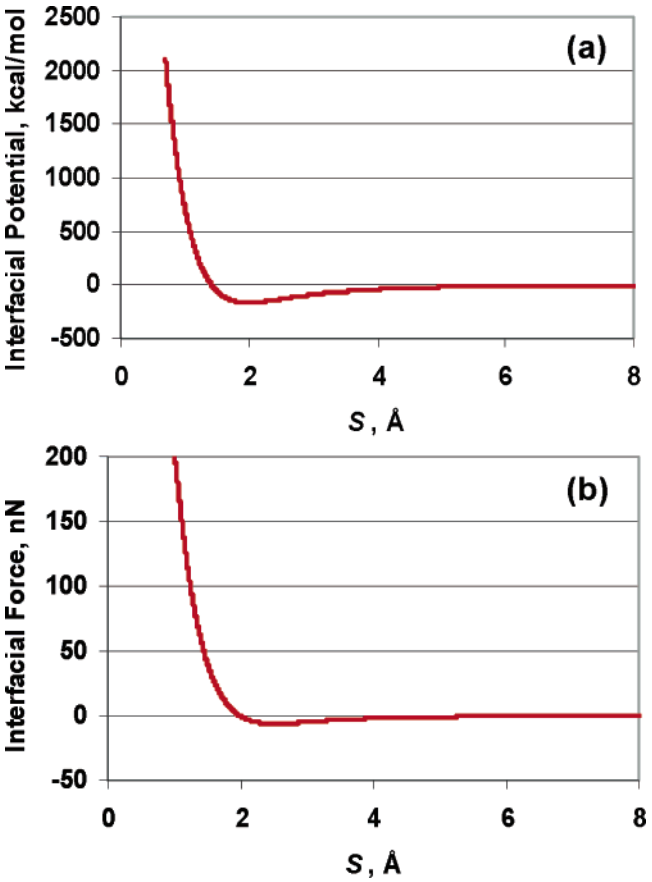

Figure 3. (a) Interfacial intermolecular potential (kcal/mol) as a function of distance, S, between the planes of the interfacial H-atom layers. Each surface is held fixed in its equilibrium geometry. (b) Force resulting from the interfacial potential.

surface, and the outermost surface layers separated so that S_{eq} equals 0.75, 1.00, and 1.25 Å. Each surface was first equilibrated at 300 K and then the surfaces are brought into contact. At the start of the two simulations for $S_{eq} = 0.75$ Å, the initial separation between the H-atom layers is 0.728 and 0.743 Å, slightly smaller than S_{eq} because of the thermal expansion of the surfaces. After the interface and surfaces have thermally equilibrated at 300 K, the average interfacial separation became 1.31 Å for each trajectory,[62] with the height of the upper surface 0.35 Å smaller than its 0 K height and the part of the bottom surface lying below the upper surface, 0.21 Å smaller than its 0 K height. At the start of the two simulations for $S_{eq} = 1.00$ Å, the initial separation between the H-atom layers is 0.978 Å and 0.993 Å. The average separation for each of the equilibrated trajectories is 1.41 Å. The two trajectories with $S_{eq} = 1.25$ Å have different initial separations of 1.228 and 1.243 Å and an identical average separation of 1.52 Å after equilibration.

For the heat transfer simulations reported below, T_{hot} for the upper surface is greater than the 300 K value for the lower surface. These simulations were performed for 52.5 ps and an average interfacial separation, S, of the H-atom layers was determined for the second half of each of these trajectories. Individual trajectories were calculated for the same simulation model as the one used above, but with $T_{hot} = 800$ K. The outermost layers were separated so that S_{eq} equals 0.75, 1.00, 1.25, 1.50, 1.75, 2.00, 2.25, 2.50, and 2.75 Å. The resulting values of S for each S_{eq} are given by the following S_{eq}, S pairs: that is, 0.75, 1.31; 1.00, 1.41; 1.25, 1.52; 1.50, 1.65; 1.75, 1.80; 2.00, 1.98; 2.25, 2.19; 2.50, 2.42; and 2.75, 2.67. It is significant that these values of S for S_{eq} of 0.75, 1.00, and 1.25 Å are the same, to within three significant figures of those given above for $T_{hot} = 300$ K. Because of the diminished interfacial repulsion, the S_{eq} and S values become similar as S_{eq} is increased. Near S_{eq} of 2.00 Å, S_{eq} and S are nearly equal as a result of the balance between the interfacial repulsion and the thermal expansion of the surfaces. For S_{eq} less than 2.00 Å, S is greater than S_{eq}. However, for S_{eq} greater than 2.00 Å, S is larger. Thermal expansion wins over interfacial repulsion for the latter S_{eq}. In addition, the repulsion between the surfaces turns into an attractive interaction for S larger than 2.00 Å.

To identify initial conditions for the different simulations presented below, S_{eq} is used to represent the distance between the outermost, fixed layers of the top and bottom surfaces. From the value of S_{eq} and the 0 K surfaces' heights given in Figure 2, the separation between the fixed, outermost layers may be determined for the trajectory simulation. The actual interfacial separations, S, found from the simulations for the different S_{eq} are given above.

B. Interfacial, Applied, and Interlayer Forces. A force was applied to the two surfaces by fixing the separation of their outermost layers as described above. This specifies the initial repulsive intermolecular potential and interfacial force between the surfaces. The upper surface is first equilibrated at temperature T_{hot}, and the lower surface is equilibrated at 300 K. They are then brought into contact with their interfacial forces turned on, their outermost layers held fixed, and their separation specified by S_{eq} as described above. The center of mass of each surface evolves in time according to Newton's equation, that is

$$F_{int} + F_{app} = M_{cm}\,\ddot{z}_{cm} \tag{5}$$

and once the simulation is initiated, the initial interfacial force relaxes and is distributed throughout the surfaces. The applied force, F_{app}, necessary to fix the positions of the atoms in the outermost layer, is the z component of the force experienced by these atoms. It is the sum of the derivatives of the surface's potential, V, with respect to the z coordinates of the atoms in the outermost layer, that is

$$F_{app} = \sum_{i}^{\text{outermost}} \frac{\partial V}{\partial z_i} \tag{6}$$

Similarly, the interfacial force, F_{int}, is a sum of all of the derivatives of the interfacial H−H, H−C, and C−C intermolecular potentials (see Section II.A), with respect to the z coordinates of the interfacial atoms in one of the surfaces. The force between two layers, of one of the surfaces, is the derivative of the interlayer potential. It may be calculated analytically as described above for F_{int} or numerically by an infinitesimal change in the interlayer separation in the z dimension.

Once a simulation is started, there is a rapid force relaxation with a decrease in F_{int} and increase in F_{app}, and then these two forces fluctuate about nearly identical average values. This is illustrated in Figure 4 for a representative trajectory with an initial separation of $S_{eq} = 1.25$ Å and $T_{hot} = 800$ K. F_{app} given in this figure is for the hot surface. Figure 4a shows that the relaxation between F_{int} and F_{app} is complete within less than 1 ps. Both F_{int} and F_{app} have periodic oscillations, whose maxima and minima are out of phase. Although the oscillations in F_{app} are much larger than those for F_{int}, when averaged from 1 to 52.5 ps, their average values are nearly identical and the same within four significant figures, that is, $\langle F_{app}\rangle = \langle F_{int}\rangle = 44.06$ nN. Figure 5 shows the C−H and C−$C_{interface}$ interlayer forces for the hot surface for 7.5 ps of motion. (The C−$C_{interface}$

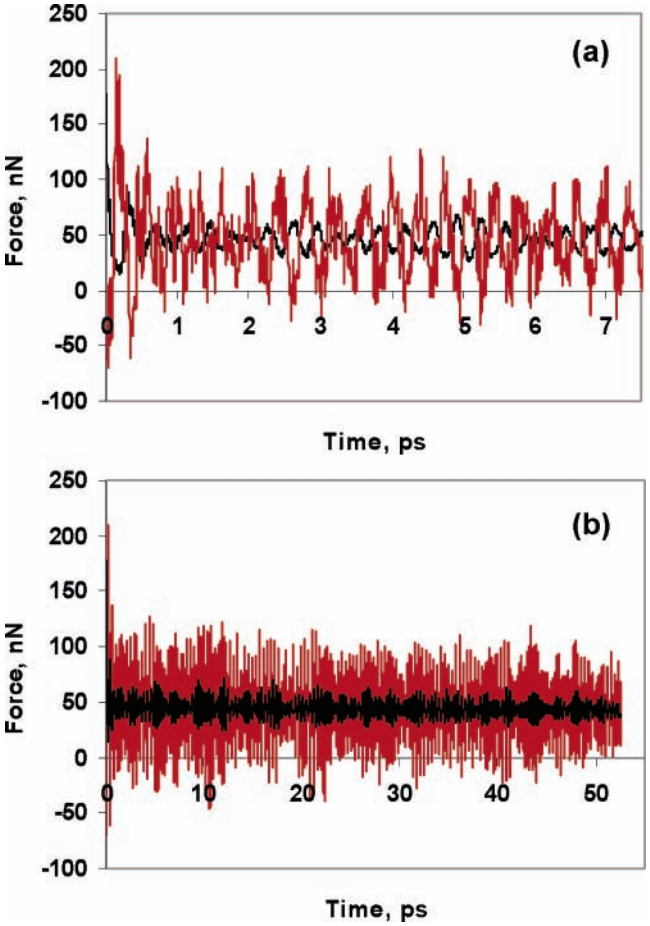

Figure 4. Interfacial force, F_{int}, (black line) and applied force, F_{app}, (red line) versus time for the hot, upper surface initially at 800 K and the cold, lower surface initially at 300 K. S_{eq} of the interfacial H-atom layers is 1.25 Å (see text) and the small interface is used for the hot surface. (a) Results for the first 7.5 ps; and (b) results for the complete 52.5 ps simulation.

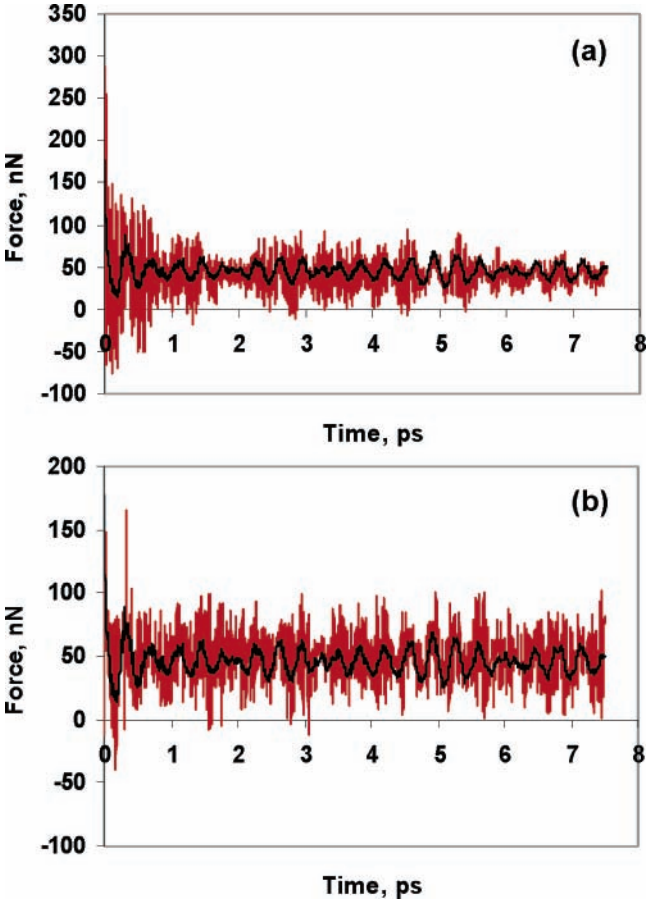

Figure 5. Interfacial force and interlayer forces for the hot surface versus time. The red line in a is the C−H interlayer force, and in b it is the C−$C_{interface}$ interlayer force. The black line in both figures is F_{int}, the interfacial force. The simulation conditions are the same as those in Figure 4. The C−$C_{interface}$ interlayer force is the force between the two closely separated C-atom layers adjacent to the H-atom interface; see Figure 1.

interlayer force is the force between the two closely separated C-atom layers adjacent to the H-atom interface; see Figure 1). These forces also rapidly relax, as found for F_{int} and F_{app}. Their average values after 1 ps are 45.88 and 45.94 nN, respectively, and nearly the same as those for $\langle F_{app}\rangle = 45.88$ and $\langle F_{int}\rangle = 45.85$ nN computed for the same period of time, from 1 to 7.5 ps.

The rapid decrease in F_{int} from its value at the beginning of the simulation to its much lower value once the surface forces relax is consistent with the increase in the interfacial separation. To illustrate this, for the two trajectories calculated at 800 K with $S_{eq} = 1.25$ Å, we found that F_{int} is 177.30−141.79 nN at the beginning of the simulation but 43.14 nN after the force relaxes. Concomitantly, the initial interfacial separation is 1.089−1.175 Å and then 1.52 Å after the force relaxation.

Figure 4 shows that there are extensive fluctuations in the interfacial force, F_{int}, at short times because of extensive surface relaxations. However, after less than 1 ps, the fluctuations become much smaller and for each trajectory F_{int} decreases *on average* in a near linear manner as represented by

$$\bar{F}(t) = \bar{F}(0) + \bar{F}'(t)t \qquad (7)$$

Here $\bar{F}(0)$ is the average interfacial force after the surface relaxations and $\bar{F}'(t)$ is the change in the average force versus time as a function of time. Values of $\bar{F}(0)$ and $\bar{F}'(t)$ were determined from simulations with S_{eq} of 0.75, 1.25, and 2.50 Å

TABLE 2: Time Dependence of the Average Interfacial Force versus Interfacial Separation[a]

parameter[b]	traj 1	traj 2	average
	$S_{eq} = 0.75$ Å		
$\bar{F}(0)$	95.409	94.947	95.178
$\bar{F}'(t)$	−0.109	−0.098	−0.104
	$S_{eq} = 1.25$ Å		
$\bar{F}(0)$	45.81	45.635	45.722
$\bar{F}'(t)$	−0.066	−0.066	−0.066
	$S_{eq} = 2.50$ Å		
$\bar{F}(0)$	−5.755	−5.706	−5.731
$\bar{F}'(t)$	-4.338×10^{-4}	-1.748×10^{-3}	-1.091×10^{-3}

[a] The simulations are for $T_{hot} = 800$ K, the H,H interface, and the small interfacial area for the hot surface. [b] $\bar{F}(0)$ is in units of nN and $\bar{F}'(t)$ is in units of nN/ps.

with $T_{hot} = 800$ K, a H,H interface, and the small interfacial area for the hot surface. The interfacial force was analyzed from 1 ps, after force relaxations are complete, to 52.5 ps. Two trajectories were calculated for each S_{eq} and the resulting values for $\bar{F}(0)$ and $\bar{F}'(t)$ are listed in Table 2. It is seen that both $\bar{F}(0)$ and $\bar{F}'(t)$ decrease with increase in S_{eq}. For $S_{eq} = 2.50$ Å, the interfacial interaction is attractive, not repulsive, and $\bar{F}(0)$ is negative. The two trajectories for an S_{eq} give very similar results, which indicates that the interfacial dynamics may be studied with a single trajectory. As discussed below, a similar finding is obtained for the dynamics of the interfacial heat transfer.

TABLE 3: Rate Constant for Heat Transfer between the Hot and Cold Surfaces versus Interfacial Properties

surface model	S_{eq} (Å)	T_{hot} (K)	H/D isotope: hot surf	H/D isotope: cold surf	hot surface area	k (ps^{-1})
standard interfacial properties						
1	0.75	800	H	H	small	0.070
1	1.00	800	H	H	small	0.055
1	1.25	800	H	H	small	0.041
1	1.50	800	H	H	small	0.031
1	1.75	800	H	H	small	0.017
1	2.00	800	H	H	small	0.0054
1	2.25	800	H	H	small	0.0018
1	2.50	800	H	H	small	0.00051
1	2.75	800	H	H	small	0.000097
effect of higher T_{hot}						
1	1.25	1000	H	H	small	0.041
1	1.25	1200	H	H	small	0.045
effect of deuterium substitution						
1	1.25	800	D	D	small	0.046
1	1.25	800	H	D	small	0.034
1	1.25	800	D	H	small	0.032
effect of larger interfacial area for hot surface						
1	1.25	800	H	H	large	0.039
effect of Model 2 for the surface potential (increased anharmonicity)						
2	0.75	800	H	H	small	0.069
2	1.25	800	H	H	small	0.037
2	1.25	1200	H	H	small	0.041
2	1.75	800	H	H	small	0.017
effect of Model 3 for the surface potential (completely quadratic)						
3	0.75	800	H	H	small	0.061
3	1.25	800	H	H	small	0.034
3	1.25	1200	H	H	small	0.031
3	1.75	800	H	H	small	0.0093

Figures 4 and 5 show that there are significant fluctuations in F_{int}, F_{app}, and the interlayer forces. They arise from the nature of the atomic-level dynamics of the nanosurfaces. Well-defined average forces are obtained, but as a result of the sizes of the nanosurfaces there are fluctuations in the interfacial, applied, and interlayer potentials, which give rise to fluctuations in their forces. The Figures show that there is a degree of periodicity in the force fluctuations, particularly on a short time scale, and this is a topic to be investigated in future work.

C. Heat Transfer Between the Hot and Cold Surfaces. In the following, the rate constant for heat transfer from the hot to cold nanosurface is determined as a function of the interfacial separation, S_{eq}, the temperature of the hot surface, H/D isotopic substitution at the interface, the interfacial area of the hot surface, and the model used for the surfaces' potential energy function. The results of the simulations are summarized in Table 3.

1. Effect of Interfacial Separation. For each simulation, the separation of the outer layers of the two surfaces is held fixed, that is, specified by the 0 K equilibrium *z*-distance S_{eq} between the H/D interfacial layers, with the surfaces in their equilibrium geometries. Figure 6a illustrates the effect of the interfacial separation on the heat transfer. In this figure, the total energy of the hot upper surface is plotted versus time for simulations with surface Model 1, $T_{hot} = 800$ K, C−H bonds at the interface, and the small interfacial area for the hot surface.

When the simulation is initiated, the interfacial potential between the two surfaces is turned on, which adds additional energy to each surface. This is illustrated in Figure 7a for a trajectory with $S_{eq} = 0.75$ Å. The initial energy, $E(0)$, of the hot, upper surface, before the interfacial potential energy is turned on, is the thermally equilibrated value of 7864 kcal/mol. However, with the interfacial potential included, the energy of the upper surface reaches a maximum value of $E_{max} = 9489$ kcal/mol at 0.15 ps. The resulting value for $E_{max} - E(0)$ is 1625 kcal/mol. A second randomly chosen molecular dynamics trajectory for $S_{eq} = 0.75$ Å gave a value of 1329 kcal/mol for $E_{max} - E(0)$. Because the diamond surface contracts with decrease in temperature, keeping the separation between the outermost layers of the surfaces constant and lowering T_{hot} decreases the initial interfacial repulsive potential. Increasing the separation between the outermost layers also lowers $E_{max} - E(0)$.

The increase in the energy of the hot, upper surface to E_{max} has only a small effect on the overall decrease in the upper surface's energy versus time. Energy transfer from the hot surface to the cold, lower surface is found to be exponential and well-fit by the expression

$$E(t) = (E_i - E_f)\exp(-kt) + E_f \qquad (8)$$

Here $E(t)$ is the energy content of the upper surface at time t, k is the rate constant for energy transfer, and E_i and E_f are additional fitting parameters. The E_i parameter allows a value for the intercept between $E(0)$ and E_{max} as shown in Figure 7a. The fitted values of E_f are very similar to the 300 K harmonic thermal energy of $3NkT$ for the upper surface; for example, for the trajectory in Figure 7, E_f is 3276 kcal/mol, whereas $3NkT$ is 3119 kcal/mol. A molecular dynamics simulation of the uncompressed upper surface gave a 300 K thermal energy of 2954 kcal/mol. Anharmonicities and nonlinearities in the upper surface's Hamiltonian arising from compression, the Morse terms, and finite displacements, makes the average thermal energy of the surface slightly different than $3NkT$.

The fits to $E(t)$ with eq 8 are shown in Figure 6a for S_{eq} values of 1.25 and 1.50 Å, and in Figure 7b for an S_{eq} value of 0.75 Å. Excellent fits to the $E(t)$ are obtained. The rate constants obtained for energy transfer from the hot surface, for S_{eq} in the range of 0.75−2.75 Å, are listed in Table 3. For surface Model

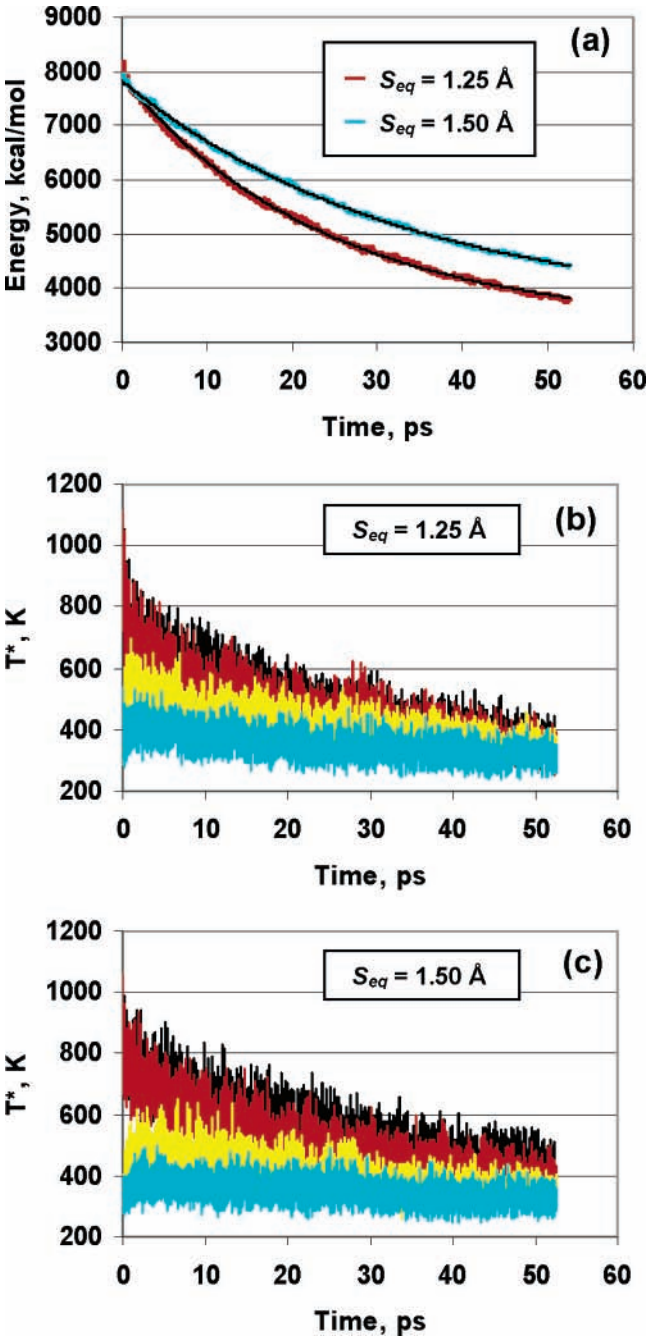

Figure 6. Results for Model 1, T_{hot} = 800 K, H-atom interface, and small interfacial area for the hot surface. (a) Total energy of the hot surface versus time for S_{eq} of 1.25 and 1.50 Å. (b) Temperature versus time for the interfacial H-atom and C-atom layers of the two surfaces with S_{eq} = 1.25 Å: red, H-hot; black, C-hot; yellow, H-cold; and blue, C-cold. (c) Same as b except S_{eq} = 1.50 Å. The interfacial C-atom layer is the one closest to the H-atom interface. The C-atom layer very close to this interfacial C-atom layer (see Figure 1) is not included.

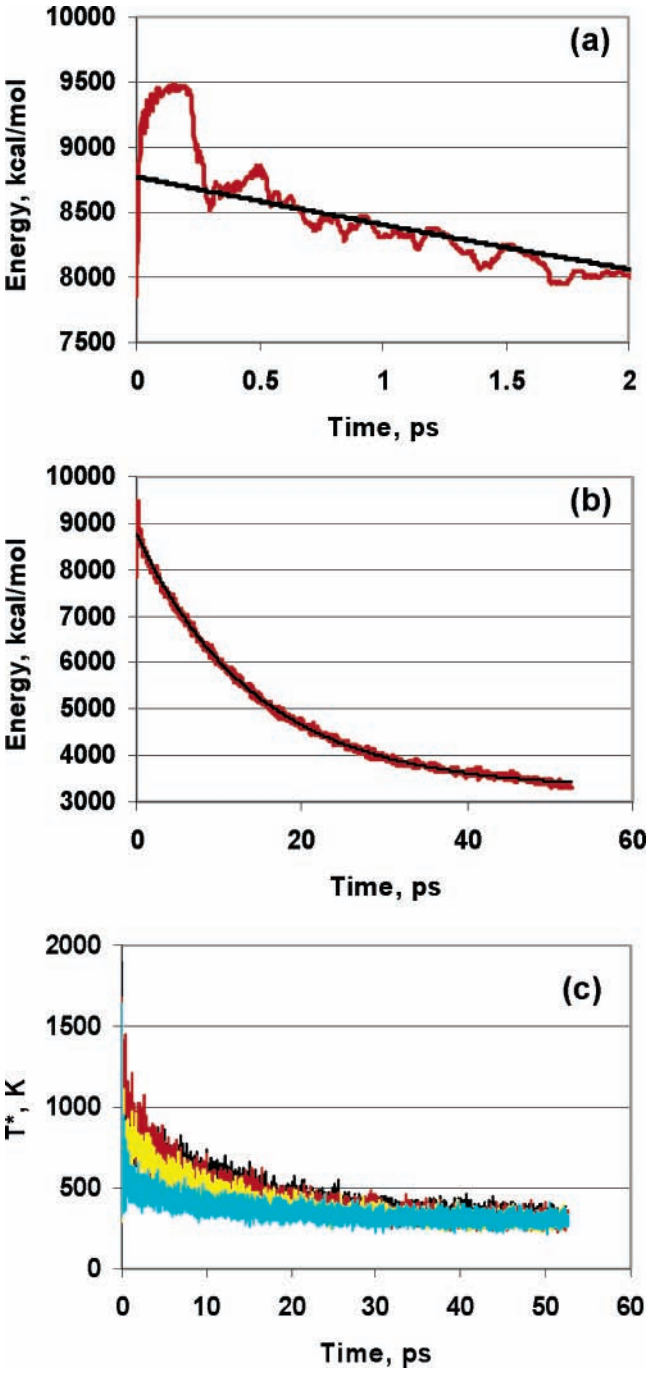

Figure 7. Simulations for S_{eq} = 0.75 Å, with Model 1, T_{hot} = 800 K, H-atom interface, and small interfacial area for the hot surface. (a) Short-time behavior of the total energy, $E(t)$, showing its increase due to the initial interfacial repulsion. (b) $E(t)$ for the complete trajectory. (c) Temperature versus time for the interfacial H-atom and C-atom layers of the two surfaces. The colors identifying the layers are given in the caption of Figure 6.

1, T_{hot} = 800 K, C−H bonds at the interface, and in the small interfacial area, the rate constant varies from 7.0×10^{-2} ps^{-1} for an S_{eq} value of 0.75 Å to 9.7×10^{-5} ps^{-1} for an S_{eq} value of 2.75 Å. Decreasing the interfacial separation and, thus, increasing the interfacial interaction enhances the rate constant for heat transfer. For S_{eq} = 2.75 Å, the interfacial interaction is very weak (see Figure 3) and the rate constant for heat transfer is very small, that is, 3 orders of magnitude smaller than that for S_{eq} = 0.75 Å. Stronger interactions between the surfaces, as a result of a smaller interfacial separation, promote equilibration of the hot surface.

Cooling and heating of layers of the hot and cold surfaces occur at different rates. This is illustrated in Figures 6b and c and 7c, where temperatures, T^*, are plotted versus time for the H-atom and C-atom interfacial layers of each surface.[63] The simulations are for S_{eq} values of 0.75, 1.25, and 1.50 Å. There is initial heating of the cold surface, which is more pronounced for the surface's H-atom layer than for the adjacent C-atom layer. For S_{eq} = 0.75 Å, there is a large interfacial force and, as shown in Figure 7c, there is rapid heating of the H-atom layer of the cold surface and thermal equilibration is complete within 52.5 ps. For the S_{eq} = 1.25 Å simulation, shown in Figure

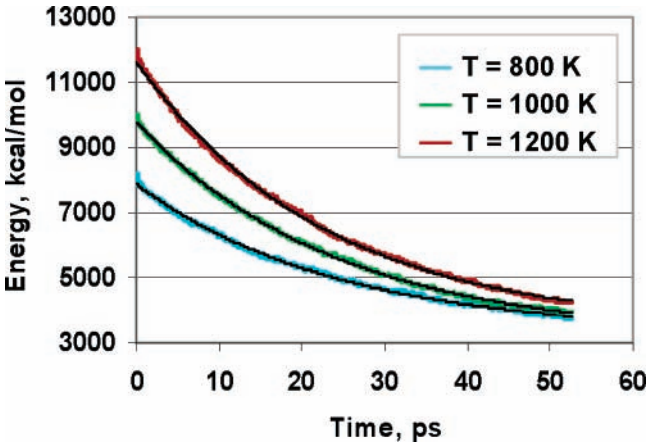

Figure 8. Total energy of the hot surface versus time for T_{hot} of 800 K (blue), 1000 K (green), and 1200 K (red). Simulation results are for Model 1, H-atom interface, small interfacial area for the hot surface, and $S_{eq} = 1.25$ Å. The black solid lines are fits by eq 8.

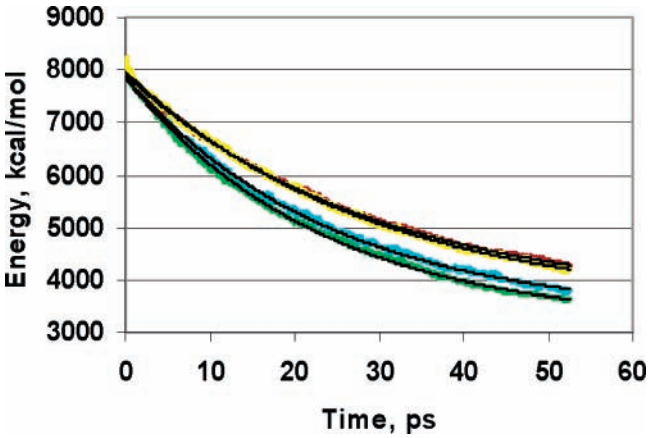

Figure 9. Total energy of the hot surface versus time for different H/D isotopic substitutions at the interface: (blue), H atoms on both surfaces; (green), D atoms on both surfaces; (yellow), H on hot surface and D on cold surface; and (red), D on hot surface and H on cold surface. Simulation results are for Model 1, $T_{hot} = 800$ K, small interfacial area for the hot surface, and $S_{eq} = 1.25$ Å. The solid lines are fits by eq 8.

6b, the temperatures of the H-atom and C-atom interfacial layers of the lower surface have begun to cool by the end of the simulation. However, equilibration is incomplete. As shown in Figure 6c, for the $S_{eq} = 1.50$ Å simulation, which has a weaker interfacial interaction, there is less initial heating of the lower surface and the upper surface remains hotter at the end of the simulation as compared to $S_{eq} = 1.25$ Å. Some differences are observed for the cooling dynamics of the interfacial H-atom and C-atom layers of the hot, upper surface. The H-atom layer cools somewhat more rapidly, which is most pronounced for the $S_{eq} = 1.50$ Å simulation.

2. Effect of Surface Temperature. Simulations were performed with the hot, upper surface at 1000 and 1200 K, instead of the 800 K investigated above, to determine how the temperature of this surface affects the rate constant for heat transfer. The same interfacial conditions as those described above were considered, with the interfacial separation, S_{eq}, set at 1.25 Å. The results of these simulations are plotted in Figure 8, where they are compared with the results for 800 K. The rate constant for heat transfer from the hot surface, determined from eq 8, is 0.041 and 0.045 ps^{-1} for 1000 and 1200 K, respectively, and statistically the same as the 0.041 ps^{-1} value at 800 K. A higher temperature gradient between the hot and cold surfaces does not have a significant effect on the rate constant for energy transfer.

3. Effect of H/D Interfacial Isotopic Substitution. The effect of H/D isotopic substitution on heat transfer between the two surfaces was studied by replacing the interfacial hydrogens of both surfaces by deuterium atoms and by replacing the hydrogens of only one of the surfaces by deuterium atoms. The simulations were performed for a temperature of 800 K and the same model for the surfaces was used as described above. The interfacial separation, S_{eq}, was set at 1.25 Å. The energies of the hot surface versus time for these simulations are shown in Figure 9, where they are compared with the result without deuteration. It is seen that replacing hydrogen by deuterium for both surfaces results in a small increase of the rate constant for heat transfer. For H atoms at the interface, k is 0.041 ps^{-1}, whereas it is 0.046 ps^{-1} with deuterium substitution. However, if the interface of the hot surface is deuterated and the cold surface is not, then the rate constant for heat transfer is substantially lower and 0.032 ps^{-1}. If the deuteration is reversed, with the cold surface deuterated and the hot surface not, then k is nearly the same and equals 0.034 ps^{-1}. Thus, a different H/D isotopic composition of the interface does not influence the energy transfer rate constant, if both surfaces have the same isotope. However, if the H/D isotopic composition of the interfaces of the two surfaces is different, then the rate of heat transfer is suppressed.

Even though the rate constants for energy transfer are nearly the same for either H or D isotopes on both surfaces, the atomistic dynamics for energy transfer is different for the two isotopes. This is illustrated in Figures 6b and 10a, where the temperatures of the interfacial H-, D-, and C-atom layers of both surfaces are plotted versus time.[63] With H atoms on both surfaces, Figure 6b, the H-atom interfacial layer of the cold, lower surface immediately heats to 600 K and equilibrates much faster with the hot surface than what occurs with D atoms on both surfaces, Figure 10a. With D atoms on the interface of the cold surface, instead of H-atoms, this surface is more "inert" with respect to receiving energy from the hot surface.

With different H/D isotopic compositions of the two surfaces, the cooling and heating of the interfacial layers depends on which surface has the H(D) isotope, as shown in Figure 10b and c. Figure 10b gives the temperature versus time for the interfacial H-, D-, and C-atom layers, with D atoms on the hot surface and H atoms on the cold surface. Although the initial energy transfer to the cold surface's H atoms is much less than what is found for the cold-surface D atoms with D atoms on both surfaces, Figure 10b shows there is some transfer with a maximum in T^* for the cold-surface H atoms at ~10 ps. However, Figure 10c shows that with H atoms on the hot surface and D atoms on the cold surface, there is no intermediate heating of the cold-surface D atoms. Temperature equilibration between the D-atom and H-atom layers is slow for surfaces with different H/D isotopes at their interface and is not attained at the end of the 52.5 ps MD simulation. The dynamics of this slow equilibration depends on which surface has the H(D) isotope.

4. Effect of Interfacial Contact Area. For the above simulations, a 22 × 20 $Å^2$ interfacial area (identified as standard) was used for the hot, upper surface. To determine whether increasing the size of this interfacial area would affect the rate constant for energy transfer, we performed a simulation with a 26 × 25 $Å^2$ interfacial area for the hot surface. The height, that is, z dimension, of this surface remained at 20 Å, and no changes were made to the size of the cold, lower surface. This larger, hot, upper surface contains 2576 atoms compared to the 1746 atoms for the standard surface model. The simulations were

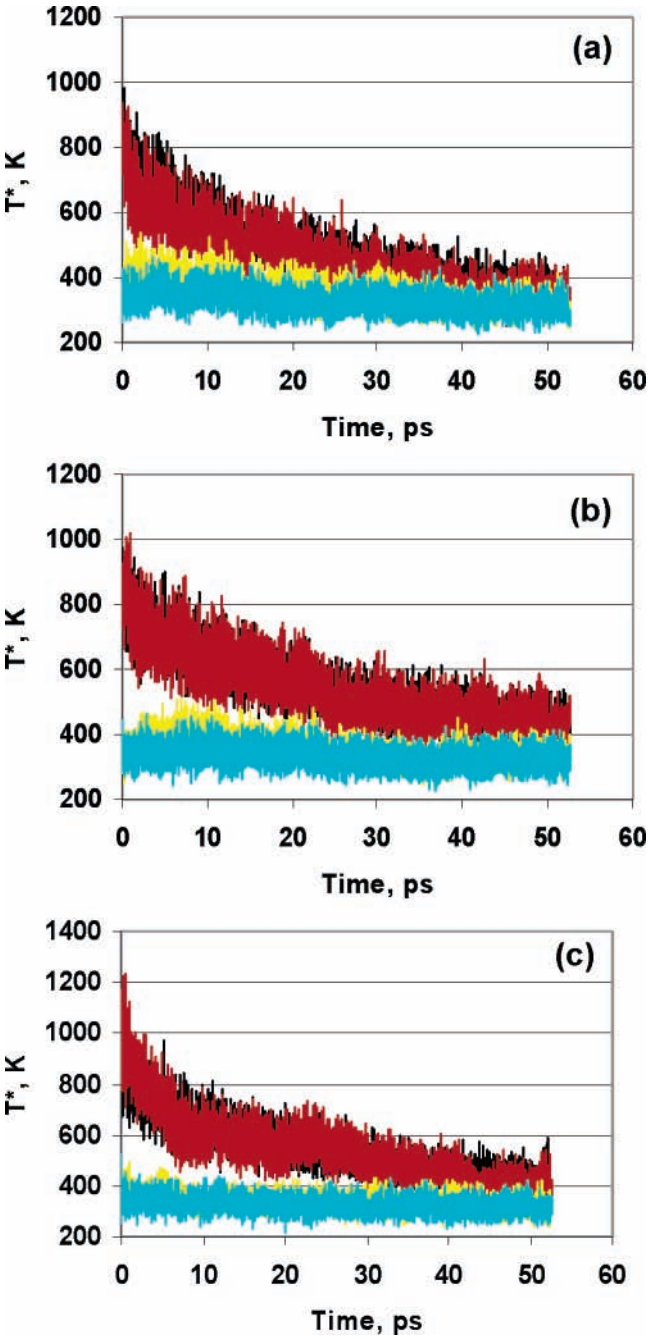

Figure 10. Effect of H/D isotopic substitutions on the temperatures of the interfacial layers. Calculations are for Model 1, $T_{hot} = 800$ K, small interfacial area for the hot surface, and $S_{eq} = 1.25$ Å. (a), D atoms on both surfaces; (b), D atoms on the hot surface and H atoms on the cold surface; and (c), H atoms on the hot surface and D atoms on the cold surface. Black and red graphs are for the interfacial C and H(D) atoms of the hot surface, respectively. Yellow and blue lines are for the H(D) and interfacial C-atoms of the cold surface, respectively.

performed for potential Model 1, $S_{eq} = 1.25$ Å, interfacial H-atoms, and $T_{hot} = 800$ K. A plot of the energy content in the hot surface versus time is given in Figure 11 where it is compared to the above result for the standard interfacial area for the hot surface. The rate constant for energy transfer from the hot surface is 0.039 ps^{-1} for the larger interface and 0.041 ps^{-1} for the standard interface. Increasing the contact area for the hot surface does not significantly affect the rate constant for energy transfer from the hot to the cold surface.

5. Effect of Varying the Model for the Surfaces' Intramolecular Potential. The above calculations were performed with

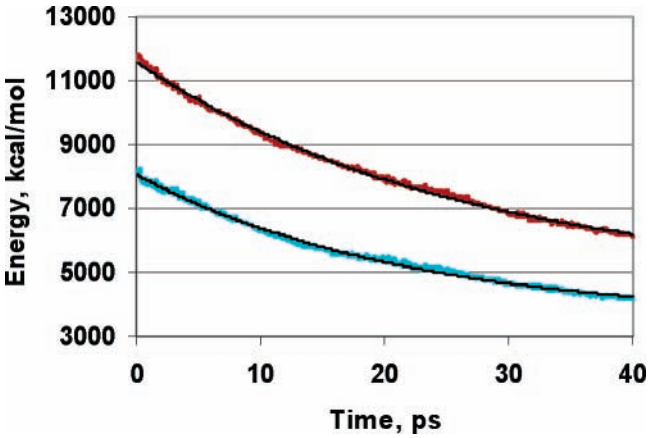

Figure 11. Total energy of the hot surface versus time for Model 1, H-atom interface, $S_{eq} = 1.25$ Å, $T_{hot} = 800$ K, and large (red) and standard (blue) interfacial areas. The solid lines are fits by eq 8.

Model 1 for the surfaces' potential energy function. It is based on the quadratic force field fit to the diamond phonon spectrum,[53,54] but with the C−C and C−H harmonic stretch terms replaced by their Morse function counterparts.[55] Models 2 and 3 were used for the surface potential to determine how variations in this potential affects energy transfer from the hot to the cold surface. Model 2 is the same as Model 1, except the diagonal bending and nondiagonal stretch−bend and bend−bend quadratic force constants were attenuated[56] as bonds defining the potential term were stretched. As shown in Table 3, the energy transfer rate constants obtained with Model 2 are nearly the same as those for Model 1. Thus, introduction of cubic and higher order anharmonic potential terms, by force constant attenuation, does not affect the rate of energy transfer.

Model 3 for the surface potential is the quadratic force field fit to the diamond phonon spectrum, without Morse functions for the C−C and C−H stretch terms and without force constant attenuation. The energy transfer rate constants obtained with this model are listed in Table 3, where it is seen that they are somewhat smaller than those determined with Models 1 and 2. The principal origin of this difference is the increased compressibility of Model 3 as compared to Models 1 and 2, which results in a greater interfacial separation for the same S_{eq} and, thus, a weaker interfacial interaction. This is illustrated by comparing the average interfacial separation for the last half of the simulation for Models 1 and 3, with $T_{hot} = 800$ K, H-atom interface, a small interface for the hot surface, and $S_{eq} = 1.25$ Å. For Model 1 this average separation is 1.52 Å, whereas it is larger and 1.56 Å for Model 3. Model 3 is more compressible because the C−C and C−H quadratic terms are not as repulsive as their Morse counterparts.

6. Effect of the Interfacial Force. As discussed above in Section III.B, after the force relaxations that occur within 1 ps are complete, the average interfacial force, F_{int}, becomes nearly constant and changes very little during a simulation. Thus, for each S_{eq} there is a well-defined $\langle F_{int} \rangle$. In Figure 12a, the rate constant, k, for energy transfer is plotted versus $\langle F_{int} \rangle$, where $\langle F_{int} \rangle$ is found by averaging the interfacial force over the last half of the 52-ps simulation. The important result in Figure 12a is the near-linear dependence of the energy transfer rate constant on $\langle F_{int} \rangle$, which varies from ~90 nN to an attractive force of ca. −6 nN. For the smallest k values, the linear relationship between k and $\langle F_{int} \rangle$ is still present as shown in Figure 12b. The slope for the plots in Figure 12a and b is 7×10^{-4} ps^{-1}/nN.

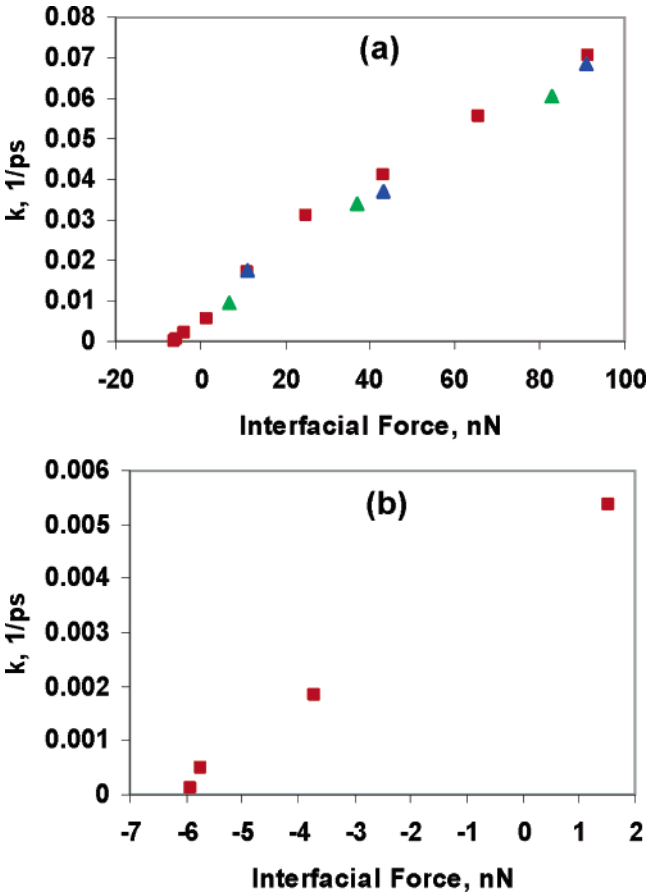

Figure 12. Plots of the rate constant for heat transfer versus interfacial force, $\langle F_{int} \rangle$. a is a linear plot for all of the data and b is a linear plot for the lowest $\langle F_{int} \rangle$. The red, blue, and green points are for surface potential Models 1, 2, and 3, respectively.

IV. Role of Quantum Dynamics

For the above simulations, with a large interfacial force and strong intermolecular interaction between the two surfaces, classical mechanics is expected to give the correct energy transfer dynamics. This is a result of the large density of states involved in the energy transfer and classically allowed pathways for the transfer. The accuracy of classical mechanics for these dynamics has been shown in comparisons between classical and quantum dynamics and/or classical dynamics and experiment for a large number of related processes.[14−17,64−73] However, quantum dynamics may become important when there is a weak interaction between the two surfaces. Here, energy transfer is expected to occur via exchange of high-energy vibrational quanta between C−H bonds of the two surfaces, with the bonds weakly coupled via van der Waals interactions.[74] For such cases, the energy transfer process may not occur classically or artificial energy transfer may occur classically via events that transfer energy amounts much less than one C−H vibrational quantum. Quantum effects have often been found to be important for translation−vibration and vibration−vibration energy transfer when the accessible number of vibrational states is sparse.[75,76]

Because of the large thermal de Broglie wavelengths for the phonon modes of a diamond lattice,[53,54] classical dynamics that assume continuous energies gives substantially greater thermal motions for the lattice than quantum dynamics does. A resulting effect of this difference is that the classical coefficient of thermal expansion is expected to be larger than the quantum value. The classical thermal expansion of the smaller upper diamond nanostructure studied here varies linearly for the temperatures in the range of 300 to 1200 K to give a thermal expansion coefficient $\gamma = [h(T) - h(300)]/h(300)$ of 3.9×10^{-6}. Here, $h(T)$ is the height of the nanostructure for temperature T. The experimental value[77] of γ for macroscopic diamond at 300 K is 1.5×10^{-6} and 2.6 times smaller than the classical value for the nanostructure. It is noteworthy that the value of γ for a diamond nanostructure will depend on the size of the structure because the phonon modes are size-dependent.[13] However, this issue was not addressed here. Of importance for the current simulations is that for a fixed outer separation of the two nanostructures, the classical interfacial separation, S, will be smaller than the quantum S as a result of the larger classical value for γ. This effect may be important for a very weak interfacial force.

In summarizing the above discussions, classical mechanics is expected to describe the interfacial dynamics correctly, except for cases in which the interfacial force is weak. Thus, for the results plotted in Figure 12, quantum effects may be important for the smallest heat transfer rate constants. Quantum dynamical calculations of heat transfer at the interface of two weakly interacting diamond nanosurfaces would be of substantial interest.

V. Summary

In the work presented here, molecular dynamics simulations are performed to study possible factors influencing the dynamics and efficiency of heat transfer across the interface of two diamond nanosurfaces. The model used for this study is one in which a small, hot surface is placed on a large, colder surface at 300 K. An important finding of the study is that relaxation of the high interfacial force initially created, when the surfaces are brought into contact, occurs on a subpicosecond time scale and much faster than the heat transfer occurs across the interface. After this force relaxation, there is a well-defined average interfacial force $\langle F_{int} \rangle$ during the simulation. The kinetics of heat transfer from the hot to the cold surface is first-order with a rate constant, k, that varies linearly with $\langle F_{int} \rangle$ according to 7×10^{-4} ps^{-1}/nN. This linear relationship is valid for all of the $\langle F_{int} \rangle$ investigated from ca. 90 nN to ca. −6 nN. Variations in the temperature and size of the hot surface, the H/D isotopic composition of the surfaces' interface, and the analytic form of the surfaces' intramolecular potentials do not have substantial effects on the rate constant, k, for heat transfer. The value of k increases by only 10% at most when the temperature of the hot nanosurface is increased from 800 to 1200 K. The rate of heat transfer increases as the interfacial area of the hot surface is increased, but k does not change. Replacing all of the interfacial H-atoms with D-atoms results in a k value only ~10% larger. However, different isotopic substitution (i.e., either H or D) on the two nanosurfaces has a more noticeable effect and decreases k by ~25% from its value with either only H or D atoms at the interface.

The results of the MD simulations for a specific $\langle F_{int} \rangle$ are independent of the three models used for the surfaces' analytic intramolecular potentials. The models varied from one with only quadratic potential energy terms to one with extensive anharmonicity arising from Morse stretches and anharmonic bends with bend−stretch coupling. These additional anharmonic terms do not affect the kinetics of heat transfer from the hot to the cold surface. A difference found for these three models is that the two with Morse stretch potentials have a slightly larger classical coefficient of thermal expansion than the model with only quadratic potential energy terms.

Acknowledgment. This research was supported by the Office of Naval Research, Department of Energy, and the Robert A. Welch Foundation. We thank Donald W. Brenner for helpful discussions.

References and Notes

(1) Oref, I.; Rabinovitch, B. S. *Acc. Chem. Res.* **1978**, *12*, 166.
(2) Hase, W. L. *J. Phys. Chem.* **1986**, *90*, 365.
(3) Uzer, T. *Phys. Rep.* **1991**, *199*, 73.
(4) Lehmann, K. K.; Scoles, G.; Pate, B. H. *Annu. Rev. Phys. Chem.* **1994**, *45*, 241.
(5) Gruebele, M.; Bigwood, R. *Int. Rev. Phys. Chem.* **1998**, *17*, 91.
(6) *Theory of Atomic and Molecular Clusters*; Jellinek, J., Ed.; Springer Series in Cluster Physics; Springer: New York, 1999.
(7) Assman, J.; von Benten, R.; Charvat, A.; Abel, B. *J. Phys. Chem. A* **2003**, *107*, 5291.
(8) Elles, C. G.; Cox, M. J.; Crim, F. F. *J. Chem. Phys.* **2004**, *120*, 6973.
(9) Campbell, D. K.; Flach, S.; Kivshar, Y. S. *Phys. Today* **2004**, *January*, 43.
(10) Bargheer, M.; Zhavoronkov, N.; Gritsai, Y.; Woo, J. C.; Kim, D. S.; Woerner, M.; Elsaesser, T. *Science* **2004**, *306*, 1771.
(11) Xie, H.; Song, K.; Mann, D. J.; Hase, W. L. *Phys. Chem. Chem. Phys.* **2002**, *4*, 5377.
(12) Gao, J.; Luedtke, W. D.; Gourdon, D.; Ruths, M.; Israelachvili, J. N.; Landman, U. *J. Phys. Chem. B* **2004**, *108*, 3410.
(13) Chen, Y.-R.; Chang, H.-C.; Cheng, C.-L.; Wang, C.-C.; Jiang, J. C. *J. Chem. Phys.* **2003**, *119*, 10626.
(14) Sibert, E. L., III; Reinhardt, W. P.; Hynes, J. T. *J. Chem. Phys.* **1984**, *81*, 1115.
(15) Page, R. H.; Shen, Y. R.; Lee, Y. T. *J. Chem. Phys.* **1988**, *88*, 4621.
(16) Lu, D.-H.; Hase, W. L. *J. Phys. Chem.* **1988**, *92*, 3217.
(17) Wyatt, R. E.; Iung, C.; Leforestier, C. *J. Chem. Phys.* **1992**, *97*, 347.
(18) Quack, M. *Annu. Rev. Phys. Chem.* **1990**, *41*, 839.
(19) Moritsugu, K.; Miyashito, O.; Kidera, A. *Phys. Rev. Lett.* **2000**, *85*, 3970.
(20) Yu, X.; Leitner, D. M. *J. Chem. Phys.* **2003**, *119*, 12673.
(21) Bu, L.; Straub, J. E. *J. Phys. Chem. B* **2003**, *107*, 12339.
(22) Wales, D. J.; Ohmine, I. *J. Phys. Chem.* **1993**, *98*, 7257.
(23) Peslherbe, D. H.; Hase, W. L. *J. Chem. Phys.* **1996**, *105*, 7432
(24) Vekhter, B.; Ball, K. D.; Rose, J.; Berry, R. S. *J. Chem. Phys.* **1997**, *106*, 4644.
(25) Miller, M. A.; Doye, J. P. K.; Wales, D. J. *J. Chem. Phys.* **1999**, *110*, 328.
(26) Braun, O.; Kivshar, Y. S. *Phys. Rep.* **1998**, *1*, 306.
(27) Yan, T.-Y.; Hase, W. L. *Phys. Chem. Chem. Phys.* **2000**, *2*, 901.
(28) Ferguson, M. K.; Lohr, J. R.; Day, B. S.; Morris, J. R. *Phys. Rev. Lett.* **2004**, *92*, 73201.
(29) Mikulski, P. T.; Harrison, J. A. *J. Am. Chem. Soc.* **2001**, *123*, 6873.
(30) Che, J.; Cağin, T.; Deng, W.; Goddard, W. A., III *J. Chem. Phys.* **2000**, *113*, 6888.
(31) Madhusudana, C. V.; Fletcher, L. S. *J. Am. Inst. Aeronaut. Astronaut.* **1986**, *24*, 510.
(32) Majumdar, A.; Tien, C. L. *Trans. Am. Soc. Mech. Eng.* **1991**, *113*, 516.
(33) Leung, M.; Hsieh, C. K.; Goswami, D. Y. *J. Heat Transfer* **1998**, *120*, 51.
(34) Wahid, S. M. S. *Int. J. Heat Mass Transfer* **2003**, *46*, 4751.
(35) Mazyar, O. A.; Xie, H.; Hase, W. L. *J. Chem. Phys.* **2005**, *122*, 094713/1−12.
(36) Harrison, J. A.; White, C. T.; Colton, R. J.; Brenner, D. W. *Thin Solid Films* **1995**, *260*, 205.
(37) Perry, M. D.; Harrison, J. A. *Thin Solid Films* **1996**, *290*−*291*, 211.
(38) Perry, M. D.; Harrison, J. A. *J. Phys. Chem. B* **1997**, *101*, 1364.
(39) Tutein, A. B.; Stuart, S. J.; Harrison, J. A. *Langmuir* **2000**, *16*, 291.
(40) Lio, A.; Charych, D. H.; Salmeron, M. *J. Phys. Chem. B* **1997**, *101*, 3801.
(41) Barrena, E.; Kopta, S.; Ogletree, D. F.; Charych, D. H.; Salmeron, M. *Phys. Rev. Lett.* **1999**, *82*, 2880.
(42) Heuberger, M.; Drummond, C.; Israelachvili, J. *J. Phys. Chem. B* **1998**, *102*, 5038.
(43) Heuberger, M.; Luengo, G.; Israelachvili, J. N. *J. Phys. Chem. B* **1999**, *103*, 10127.
(44) Drummond, C.; Israelachvili, J. *Phys. Rev. E.* **2001**, *63*, 041506.
(45) Demirel, A. L.; Granick, S. *J. Chem. Phys.* **1998**, *109*, 6889.
(46) Ruth, M.; Granick, S. *J. Phys. Chem. B* **1999**, *103*, 8711.
(47) Demirel, A. L.; Granick, S. *J. Chem. Phys.* **2002**, *117*, 7745.
(48) Klein, J.; Kumacheva, E. *J. Chem. Phys.* **1998**, *108*, 6996.
(49) Kumacheva, E.; Klein, J. *J. Chem. Phys.* **1998**, *108*, 7010.
(50) Mate, C. M.; Arnett, P. C.; Baumgart, P.; Dai, Q.; Guruz, U. M.; Knigge, B. E.; Payne, R. N.; Ruiz, O. J.; Wang, G. J.; Yen, B. K. *IEEE Trans. Magn.* **2004**, *40*, 3156.
(51) Mugele, F.; Salmeron, M. *J. Chem. Phys.* **2001**, *114*, 1831.
(52) Tabor, D.; Field, J. E. In *The Properties of Natural and Synthetic Diamond*; Field, J. E., Ed.; Academic Press: London, 1992; p 547.
(53) Tubino, R.; Piseri, L.; Zerbi, G. *J. Chem. Phys.* **1972**, *56*, 1022.
(54) Hass, K. C.; Tamor, M. A.; Anthony, T. R.; Banholzer, W. F. *Phys. Rev. B* **1992**, *45*, 7171.
(55) de Sainte Claire, P.; Barbarat, P.; Hase, W. L. *J. Chem. Phys.* **1994**, *101*, 2476.
(56) Wolf, R. J.; Bhatia, D. S.; Hase, W. L. *Chem. Phys. Lett.* **1986**, *132*, 493.
(57) Hu, X.; Hase, W. L. *J. Phys. Chem.* **1989**, *93*, 6029.
(58) Bunker, D. L. *J. Chem. Phys.* **1962**, *37*, 393.
(59) Williams, D. E.; Starr, T. L. *Comput. Chem.* **1977**, *1*, 173.
(60) Hase, W. L.; Duchovic, R. J.; Hu, X.; Komornicki, A.; Lim, K. F.; Lu, D.-h.; Peslherbe, G. H.; Swamy, K. N.; Vande Linde, S. R.; Varandas, A.; Wang, H.; Wolf, R. J. *QCPE Bull.* **1996**, *16*, 671.
(61) Berendsen, H. J. C.; Postma, J. P. M.; van Gunsteren, W. F.; DiNola, A.; Haak, J. R. *J. Chem. Phys.* **1984**, *81*, 3684.
(62) With $T \neq 0$ K for the temperatures of the surfaces, the interfacial separation is calculated as the difference between the average *z*-coordinate value for the H atoms of the upper surface and the same average for the H atoms of the lower surface.
(63) The temperatures of the interfacial layers are identified by T^* to differentiate them from the Boltzmann temperature, T, because it was not determined whether the velocity distributions for the atoms in the layers conform to Boltzmann distributions; see the discussion in ref 35.
(64) Pattengill, M. D. In *Atom-Molecule Collision Theory*; Bernstein, R. B., Ed.; Plenum: New York, 1979; p 359.
(65) Lim, K. F. *J. Chem. Phys.* **1994**, *100*, 7385.
(66) Liu, J.; Song, K.; Hase, W. L.; Anderson, S. L. *J. Chem. Phys.* **2003**, *119*, 3040.
(67) Meroueh, O.; Hase, W. L. *Phys. Chem. Chem. Phys.* **2001**, *3*, 2306.
(68) Isa, N.; Gibson, K. D.; Yan, T.; Hase, W. L.; Sibener, S. J. *J. Chem. Phys.* **2004**, *120*, 2417.
(69) Hase, W. L.; Buckowski, D. G.; Swamy, K. N. *J. Phys. Chem.* **1983**, *87*, 2754.
(70) Untch, A.; Schinke, R.; Cotting, R.; Huber, J. R. *J. Chem. Phys.* **1993**, *99*, 9553.
(71) Wang, H.; Peslherbe, G. H.; Hase, W. L. *J. Am. Chem. Soc.* **1994**, *116*, 9644.
(72) Baer, T.; Hase, W. L. *Unimolecular Reaction Dynamics. Theory and Experiment*; Oxford: New York, 1996.
(73) Schinke, R. *Photodissociation Dynamics*; Cambridge: New York, 1993.
(74) Jucks, K. W.; Miller, R. E. *J. Chem. Phys.* **1988**, *88*, 6059.
(75) Yardley, J. T. *Introduction to Molecular Energy Transfer*; Academic: New York, 1980.
(76) Shin, H. K. In *Dynamics of Molecular Collisions, Part A*; Miller, W. H., Ed.; Plenum: New York, 1976; p 131.
(77) Novikova, S. I. *Fiz. Tverd. Tela* **1961**, *2*, 1617. (*Soviet Physics* − Solid State, **1961**, *2*, 1464).